Taylor & Francis
Taylor & Francis Group

Mathematics in Medical and Life Sciences

ISSN: 2993-7574 (Online) Journal homepage: www.tandfonline.com/journals/tmls20

Accessing the pharmacokinetics of magnetic nanoparticles in cirrhosis-associated hepatocarcinogenesis by ordinary differential equation modeling and AC biosusceptometry

Diego S. Rodrigues, Guilherme A. Soares, Verónica A. González-López, Anibal T. Bezerra, Mats Jirstrand & José R. A. Miranda

To cite this article: Diego S. Rodrigues, Guilherme A. Soares, Verónica A. González-López, Anibal T. Bezerra, Mats Jirstrand & José R. A. Miranda (2024) Accessing the pharmacokinetics of magnetic nanoparticles in cirrhosis-associated hepatocarcinogenesis by ordinary differential equation modeling and AC biosusceptometry, Mathematics in Medical and Life Sciences, 1:1, 2391739, DOI: 10.1080/29937574.2024.2391739

To link to this article: https://doi.org/10.1080/29937574.2024.2391739

MATHEMATICS IN MEDICAL AND LIFE SCIENCES
2024, VOL. 1, NO. 1, 2391739
https://doi.org/10.1080/29937574.2024.2391739

Taylor & Francis
Taylor & Francis Group

Accessing the pharmacokinetics of magnetic nanoparticles in cirrhosis-associated hepatocarcinogenesis by ordinary differential equation modeling and AC biosusceptometry

Diego S. Rodrigues [a], Guilherme A. Soares [b], Verónica A. González-López [c], Anibal T. Bezerra [d], Mats Jirstrand [e] and José R. A. Miranda [b]

[a]Faculdade de Tecnologia, Universidade Estadual de Campinas, Limeira, SP, Brazil; [b]Instituto de Biociências, Universidade Estadual Paulista "Júlio de Mesquita Filho", Botucatu, SP, Brazil; [c]Instituto de Matemática, Estatística e Computação Científica, Universidade Estadual de Campinas, Campinas, SP, Brazil; [d]Instituto de Ciências Exatas, Universidade Federal de Alfenas-MG, Alfenas, MG, Brazil; [e]Fraunhofer-Chalmers Research Centre for Industrial Mathematics, Gothenburg, Sweden

ABSTRACT

Pharmacokinetic studies using mathematical modeling examine the distribution of substances in multiple organs and compartments over time. Accordingly, this paper investigates the effect of cirrhosis-associated hepatocarcinogenesis on the pharmacokinetics of magnetic nanoparticles (MNPs) by using an *in vivo* model of cancer progression. To this end, a multichannel AC biosusceptometry system was used to record the transit of MNPs, in the heart and the liver, in two groups of animals: control (SAL), and within the diethylnitrosamine/thioacetamide-induced model of hepatocarcinogenesis (DEN/TAA). The evolution of MNPs concentration is then robustly described as a compartmental model, considering the transfer rate of nanoparticles from the heart to the liver (k_1), their return from the liver to the heart through the circulatory system (k_2), and their irreversible uptake by Kupffer cells within a liver subcompartment (k_3). Our nonlinear mixed-effects parameter estimation modeling shows that k_2 and k_3 change between SAL and DEN/TAA groups, but not k_1, indicating that cirrhosis-associated hepatocarcinogenesis is likely to affect mainly liver pharmacokinetics. Correspondingly, this is precisely reported here by also presenting a covariance analysis and an inter-individual variation of the transfer rates of the magnetic nanoparticles, contributing to their development in theranostic applications and tailored drug delivery systems.

PLAIN LANGUAGE SUMMARY

Developing effective ways to diagnose and treat disease is a fundamental area of applied sciences. To this end, nanosized particles capable of interacting with external fields, such as magnetic nanoparticles (MNPs), are a valuable tool for studying drug dynamics in biological systems. In conjunction with alternating current biosusceptometry (AC biosusceptometry), MNPs can track biodistribution processes in real-time *in vivo* experiments, allowing high temporal resolution and providing reliable data for modeling. Carcinogenic processes, such as cirrhosis-associated hepatocarcinogenesis, can alter these dynamics, adding a layer of complexity to the analysis. Detecting and quantifying these changes is not a straightforward task, especially in the presence of diseases and carcinogenic processes. Here, we present the construction of a robust modeling framework to characterize the kinetics and distribution of MNPs to improve the predictive capabilities of such theranostic delivery systems. As a result, our analysis shows that the transfer rates of MNPs across the liver is significantly sensitive to cirrhosis-associated hepatocarcinogenesis, contributing to more efficient, accurate and dedicated theranostic applications to early stages of cancer development.

ARTICLE HISTORY
Received 13 April 2024
Revised 1 August 2024
Accepted 7 August 2024

KEYWORDS
Nonlinear mixed effects models; NLMEModeling package; parameter estimation of ordinary differential equations; pharmacokinetic modeling

1. Introduction

Magnetic nanoparticles (MNPs) have been explored as a new potential theranostic agent, and several studies devoted significant efforts to employing MNPs in biomedical applications. MNPs have been used in cell separation, for magnetic particle imaging [1], as contrast agents in magnetic resonance imaging (MRI) [2], and for magnetic hyperthermia [3]. There are different measurement techniques to determine the magnetic properties of MNP. The linear dynamic magnetic susceptibility of MNP is commonly characterized by measuring their magnetization response as a function of frequency in alternating magnetic fields at low amplitudes (to ensure linearity) using alternating current (AC) susceptometer devices.

CONTACT Diego S. Rodrigues diego.rodrigues@ft.unicamp.br, diegosr@unicamp.br R. Paschoal Marmo, 1888, 13484-332, Limeira-SP, Brazil

Over the years, the Alternating Current Biosusceptometry (ACB) system has been used in numerous studies to evaluate physiological and pharmacokinetic parameters, either through animal models or even in humans [4]. Currently, the ACB system includes studies evaluating MNP in biological systems [5–7]. The system behaves like a magnetic material detector through an arrangement of coils that can be used in *in vitro* and *in vivo* assessments. Within different ACB system setups, the multichannel ACB system (MC-ACB) allows dynamic acquisitions of the distribution of MNP in real-time with a high temporal resolution [8]. Besides, MC-ACB can reconstruct MNP content *in vitro* and quantify biodistributions of MNPs in animals [8].

To ensure the non-toxicity and safety of MNPs, its pharmacokinetics is one of the main concerns when applied to *in vivo* experiments and clinical procedures. Intrinsic characteristics of MNPs result in affinity or repulsion to specific tissues, organs, or systems, requiring pre-clinical characterization studies, which aim to elucidate the relationships between the structure and activity of MNPs within an organism. For example, it is known that once the nanoparticles enter the body, the interaction with the immune system results from the particle opsonization upon contact with blood and plasma proteins. Following opsonization, the nanoparticles are quickly recognized and captured by the mononuclear phagocyte system, which consists of monocytes and macrophages, especially from the liver and spleen. Nanoparticles larger than 200 nm are sequestered by filtration in the spleen, whereas nanoparticles smaller than 6 nm are rapidly removed from the blood via renal clearance. Nanoparticles with diameters between 6 and 200 nm are preferentially captured by the Kupffer cells in the liver. As the evidence shows a high accumulation of the MNPs in the liver, the MNPs present a significant potential to be used as a contrast agent to imaging modalities such as the ACB system [8–10].

From the development of nanotechnology, MNPs have emerged as an alternative tool to conventional strategies [11–13] to be used as multifunctional probes for diagnosis and treatment aimed at liver diseases [14–18]. In this perspective, as of particular interest here, and as a major risk factor for liver cancer, hepatic cirrhosis is a disease that affects the liver due to repetitive lesions not treated over a long period, generated by chronic alcohol consumption and diseases such as hepatitis C. The disseminated fibrotic state characterizes cirrhosis, the appearance of nodules in the tissue, and micro-fistulas between afferent and efferent vessels, determining the non-reversibility of lesions [19, 20].

To reach the real translational potential of MNPs, their biodistribution must be better understood from the point of view of their systemic pharmacokinetics. Pharmacokinetic studies based on mathematical modeling consist of assessing molecule distribution among various compartments of the biological system over time, elucidating physiology and generally establishing an essential descriptive and predictive tool to investigate and understand the rates of absorption, distribution, metabolism, and excretion [21].

Compartment modeling is required in pharmacokinetics due to specific physiological processes in body organs. The association between theoretical and experimental assessments can result in a more complete and valuable tool to fully comprehend the biological process and predict the MNP pharmacokinetics [22]. Other than Dogra et al. [22], we refer to the works of Sousa-Junior et al. [23], Celechovska [24] and Baleanu et al. [25] as examples of valuable studies in pharmacokinetic modeling that use *in vivo* data and deserve to be cited as our sources of inspiration for the present work. Since we are interested in possible differences in MNPs pharmacokinetics caused by hepatocarcinogenesis, we refer to the similar work of Berglund et al. [26] as a valuable example of a study where two groups of individuals (case and control) are evaluated and compared for changes in pharmacokinetics caused by hepatocarcinogenesis. The calculated results accurately estimate the MNP parameter pharmacokinetics, comprising a realistic outcome when compared with experimental data.

Through a mathematical modeling perspective, here we address the *in vivo* biodistribution of MNPs detected by the MC-ACB system, and how the pharmacokinetics of the MNPs is affected by cirrhosis-associated hepatocarcinogenesis. Accordingly, to quantitatively describe how this disease may change the biodistribution of MNPs, two different groups of animals are addressed here: a control group with healthy animals and a group of individuals in which the process of hepatocarcinogenesis has been started [27]. This assessment was already presented in another paper [9], but not in terms of pharmacokinetic modeling. Here we fill this gap by introducing a simple ordinary differential equation (ODE) model to access changes in the pharmacokinetics of MNPs caused by the initiation of hepatocarcinogenesis.

2. Methods

2.1. Diethylnitrosamine/thioacetamide-induced hepatocellular carcinoma model

Our experimental data is derived from the diethylnitrosamine/thioacetamide-induced rat model of cirrhosis-associated hepatocarcinogenesis [9]. Regarding the

relevance of this preclinical biological model, it is important to highlight that the diethylnitrosamine (DEN) and thioacetamide (TAA)-induced liver injury model is a widely used tool for studying cirrhosis-associated hepatocarcinogenesis due to its ability to replicate many critical aspects of human disease. This model is essential as it faithfully mimics preneoplastic lesions, cellular proliferation, and tumor development in a cirrhotic environment, including increased collagen deposition and hepatocyte proliferation, reflecting the progression of the disease in humans [28]. Furthermore, the model enables in-depth examination of molecular and biochemical alterations associated with hepatocarcinogenesis, such as the upregulation of genes related to extracellular matrix deposition and the reduction in antioxidant enzyme activity, which are crucial aspects of disease progression [29, 30].

The flexibility and experimental control offered by animal models like DEN/TAA are of great importance, as they allow a high degree of control over experimental conditions. This facilitates the reproducibility of results and detailed investigation of underlying pathological mechanisms [31]. Although the observation that only 20% of animals develop hepatocellular carcinoma (HCC) might be seen as a limitation, this rate is representative of the clinical reality, where only a fraction of patients with cirrhosis develop HCC. Thus, the model mimics the natural progression of the disease, being relevant for studying the factors that contribute to disease progression [32].

The variability in the animals' response to chemical treatment can provide valuable insights into the heterogeneity of the response to liver damage and the progression to HCC. This is fundamental for identifying risk factors and protective mechanisms relevant to translational medicine [33]. Furthermore, the low incidence of HCC in a chemically induced cirrhotic context better reflects the pathogenesis observed in humans, where not all patients with cirrhosis develop liver cancer. Studies have shown that the DEN/TAA model presents molecular and histological characteristics that closely resemble human hepatocarcinogenesis [32].

2.2. In Vivo experiments with magnetic nanoparticles by alternate current biosusceptometry

In this study, we utilized signals acquired from the MC-ACB system of a published work [9]. As reported in ref. [9], all animal experiments were previously approved and performed following the recommendations issued by the National Council for Control of Animal Experimentation (CONCEA) and were approved by the Ethics Committee on Animal Use of the São Paulo State University (IBB/UNESP) under protocol 7571041120. The MC-ACB system was designed to monitor the circulation of MNPs due to its high temporal resolution and suitability for dynamic acquisitions. Using it, we simultaneously recorded the passage of MNPs in the heart and their accumulation in the liver. From these signals, we reconstructed the biodistribution of MNPs through quantitative sequential images at a sampling frequency of 20 Hz. We selected regions of interest (ROIs) from these images representing the heart and liver regions, as detailed in [9]. By recording the heart region, we assessed MNPs in the bloodstream while mapping their accumulation in the abdomen. Additionally, we also employed a second ACB setup to quantify the final mass of MNPs accumulated in the liver after the animal's death [10]. The data used for fitting the model is available upon reasonable request.

2.2.1. Magnetic nanoparticles (MNPs)

The complete characterization of the MNPs can be found at [34]. These have proven adequate over the years, presenting an excellent low-field magnetic response to ACB systems. As explored here, the association of the MNP as a tracer agent and the ACB system has enabled several evaluations of physiological processes under healthy and unhealthy conditions [7].

2.3. Mathematical modeling

In order to describe how the condition of hepatocarcinogenesis may change the pharmacokinetics of MNPs, here we address a SAL (control) group composed of signals of 9 healthy rats and a DEN/TAA (case) group composed of signals of 8 animals in hepatocarcinogenesis. These signals were selected from larger groups of animals of a previous study [9] as useful representative signals for our purpose of pharmacokinetic modeling. To describe how the pharmacokinetics of the MNP is affected by hepatocarcinogenesis, we propose the following ODE model (see Figure 1):

$$\begin{cases} \dfrac{\mathrm{d}}{\mathrm{d}t}\,(x/V_1) = -k_1\,(x/V_1) + k_2(y/V_2), & (1)\\ \dfrac{\mathrm{d}}{\mathrm{d}t}\,(y/V_2) = \quad k_1\,(x/V_1) - k_2\,(y/V_2) - k_3\,(y/V_2), & (2)\\ \dfrac{\mathrm{d}}{\mathrm{d}t}\,(z/V_2) = \quad k_3\,(y/V_2), & (3) \end{cases}$$

where $x = x(t)$, $y = y(t)$ and $z(t)$ are the amounts of the MNPs in each compartment: $x(t)$ refers to the heart, and $y(t)$ plus $z(t)$ refers to the liver, being $z(t)$ its subcompartment [22]. Regarding the parameters, k_1, k_2 and k_3 are the transfer rates between compartments (expressed in units of 1/seconds), and V_1 and V_2 are hypothetical volumes of the compartments, V_1 for the heart and V_2 for the liver (usually expressed in units of

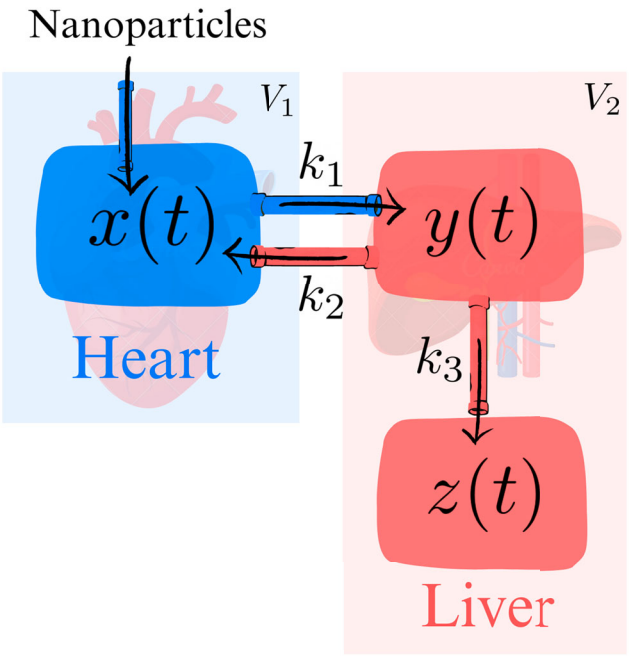

Figure 1. Schematics of the compartment model for the MNPs biodistribution.

milliliters). Thus, the model is formulated using concentrations of MNPs.

We hypothesize that the parameters of the mathematical model should be statistically different between the SAL (control) and DEN/TAA (case) groups. To test this hypothesis against experimental data, besides individual fittings for each signal, we proceed with parameter estimation at a populational level for each group. By using the measured data for both $x(t)/V_1$ and $(y(t)+z(t))/V_2$ our goal is twofold: (1) to accurately describe the biodistribution of MNPs at the individual level and (2) to use such a description at the group level to access possible relevant changes in the distribution of MNPs caused by the process of cirrhosis-associated hepatocarcinogenesis.

It is essential to emphasize that the system given by the Equations (1), (2) and (3) is very similar to the model proposed by Watt & Young [35], applied and studied in even more details by Celechovska [24], and used by Baleanu et al. in a setting of fractional derivatives [25]. The last two studies also include parameter estimation relying upon experimental data. However, in our case, we also have the compartmental volumes V_1 and V_2 appearing explicitly as parameters of the Equations (1), (2), (3). Besides accessing different parameters for each of the experimental groups (DEN/TAA and SAL), we emphasize to the reader that these volumes are key elements of our work in terms of achieving suitable fittings.

To estimate the parameters of the model, we use the Nonlinear Mixed Effects Modeling (NLME) implemented in the Mathematica® package `NLMEModeling` [36–38]. To avoid non-identifiability in the parameter estimation process, and considering that available measured data are for the quantities $x(t)/V_1$ and $(y(t)+z(t))/V_2$, we expressed the model in terms of the volume ratio $V_R = V_2/V_1$. The parameters V_2 and V_1 cannot be estimated separately because in such a case the model is not identifiable. This need of estimating the ratio $V_R = V_2/V_1$ to reach parameter identifiability was confirmed using `IdentifiabilityAnalysis` [39–42]. For the sake of clarity, the model we used in our fittings was the following:

$$\begin{cases} \dfrac{\mathrm{d}}{\mathrm{d}t}x &= -k_1\,x + k_2\,y/V_R, & (4)\\ \dfrac{\mathrm{d}}{\mathrm{d}t}y &= k_1\,x\,V_R - k_2\,y - k_3\,y, & (5)\\ \dfrac{\mathrm{d}}{\mathrm{d}t}z &= k_3\,y. & (6) \end{cases}$$

To proceed with parameter estimation, two elements are needed to use the NLME approach: an observation model for the errors of our observables $x(t)/V_1$ and $(y(t)+z(t))/V_2$ (coded in the matrix $\Sigma_{2\times2}$), and a structure of covariance for the parameters k_1, k_2, k_3, V_R (specified as the matrix $\Omega_{4\times4}$). The latter establishes random effects η_i for the parameters due to the individual variability within a population group such that $\eta_i \sim \mathcal{N}(0,\Omega)$, i.e. a multivariate normal distribution with zero mean and covariance matrix Ω.

For the covariance matrix of the residual error, we assume a quite general form, based on proportional and additive errors with unknown parameters s_1 and s_2 for $x(t)$ and unknown s_3 and s_4 for $y(t)+z(t)$:

$$\Sigma = \begin{pmatrix} [s_1\,x(t)]^2 + s_2^2 & 0 \\ 0 & [s_3(y(t)+z(t))]^2 + s_4^2 \end{pmatrix}. \quad (7)$$

For the covariance matrix of the random effects (Ω), to not impose a closed form, we assume non-zero covariance between the random effects of each parameter (k_1, k_2, k_3, and V_R). Regarding data, the individual time series comprises the initial condition plus 60 points, each point taken each 5 seconds (times $0, 5, 10, 15, \ldots, 300$). These are the original raw data signals for the heart and liver with no filtering.

Based on extensive numerical tests, we claim that the data for the heart or the liver cannot be simultaneously fitted without the use of compartmental volumes. This way, the parameter V_R is the missing degree of freedom needed for fitting the data measured both at the heart and liver compartments. The raising of this additional degree of freedom generated by V_R can be understood by inspecting the analytical solution of our ODE

system (4), (5), (6) in the specific case for which $x(0) = x_0$ and $y(0) = z(0) = 0$:

$$\begin{cases} x(t) = x_0 \dfrac{\mathrm{e}^{-p\,t}\left[(2\,k_1 - k_s)(1-\mathrm{e}^{r\,t}) + r(1+\mathrm{e}^{r\,t})\right]}{2\,r}, & (8) \\ y(t) = x_0 \dfrac{k_1\,\mathrm{e}^{-p\,t}(\mathrm{e}^{r\,t}-1)}{r}\,V_\mathrm{R}, & (9) \\ z(t) = x_0 \dfrac{\mathrm{e}^{-p\,t}\left[2\,r\mathrm{e}^{p\,t} - k_s(\mathrm{e}^{r\,t}-1) - r(1+\mathrm{e}^{r\,t})\right]}{2\,r}\,V_\mathrm{R}, & (10) \end{cases}$$

where

$$\begin{cases} k_s \doteq k_1 + k_2 + k_3 > 0, & (11) \\ r \doteq (k_s{}^2 - 4\,k_1\,k_3)^{1/2},\ k_s{}^2 - 4\,k_1\,k_3 > 0, & (12) \\ p \doteq (k_s + r)/2 > 0. & (13) \end{cases}$$

since $k_s{}^2 - 4\,k_1\,k_3 = (k_1+k_2+k_3)^2 - 4\,k_1\,k_3 = (k_1-k_3)^2 + k_2^2 + 2\,k_1\,k_2 + 2\,k_2\,k_3 > 0$.

We note that the parameter V_R appears as a simple scale factor in Equations (9) and (10), related to the liver, but not in Equation (8), which refers to the heart. Therefore, changes in the parameter V_R do not affect the value of $x(t)$, thus generating the additional degree of freedom required to obtain proper fittings of the model to experimental data.

3. Results

In another work, a classical pharmacokinetic statistical assessment is used to investigate the circulation and distribution of MNPs within the body [9]. Building upon these findings, here we use a pharmacokinetic modeling approach to provide a deeper understanding of the transfer rates of MNPs between the liver and circulating blood. Our analysis is focused on the kinetic parameters k_1, k_2, k_3, and also on the volume ratio for the liver, V_R. Our motivation here is to detect possible changes in the pharmacokinetics of MNPs due to the cirrhosis-associated hepatocarcinogenesis. As described in the preceding section, this is addressed here by fitting the parameters of the ODE system given by the Equations (4), (5), (6) for two groups: DEN/TAA (case), and SAL (control).

Regarding the MNP pharmacokinetics, in Figure 2 we report the value of each kinetic parameter (k_1, k_2, k_3) as an average and respective standard error bars within each group (SAL or DEN/TAA). Remarkably, we show that both k_2 and k_3 are found to be different between groups, but not k_1. This is consistent with the fact that the MNP liver pharmacokinetics is expected to be affected by the chemically-induced cirrhosis-associated hepatocarcinogenesis of the DEN/TAA. Regarding k_1, although the respective group averages seem to be different between

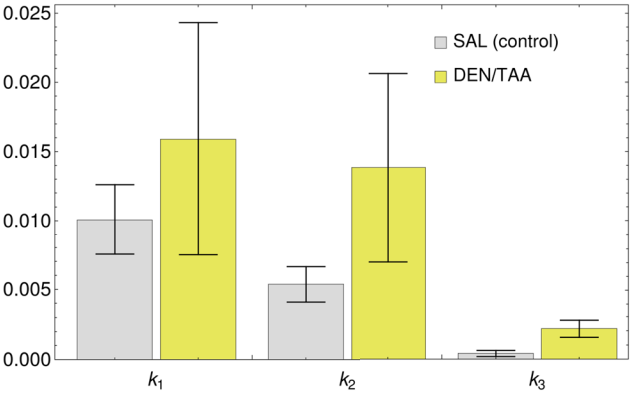

Figure 2. Averages and respective standard errors for k_1, k_2, k_3 in SAL and DEN/TAA groups.

SAL and DEN/TAA, there is a complete overlap of the estimated intervals such that significant differences cannot be attested for this parameter. This is consistent with the fact that k_1 is a transfer rate of MNP leaving the heart (compartment $x(t)$) and that k_2 and k_3 are transfer rates of MNP leaving the liver (compartment $y(t)$ plus the subcompartment $z(t)$). These latter parameters are shown to be affected by cirrhosis-associated hepatocarcinogenesis.

For the sake of completeness, and to directly illustrate the capability of our modeling in describing experimental data, we show one of the calibrated individual fittings in Figure 3. The other curves also fit the respective experimental data accordingly.

In addition to Figure 2, besides average values and standard errors for SAL and DEN/TAA, we also report the relative standard errors (RSE) and the inter-individual variabilities (IIV) for all the parameters in Table 1. According to the population modeling literature, it is established that RSE $< 30\%$ is considered good and that RSE around 50% also appears quite often [43–45]. However, this highly depends on sample size [43]. In our study, we have less than 10 individuals in each group, and then we argue that our RSEs are acceptable [43]. Considering that each group is composed of less than ten individuals, and given the fact we are estimating all the parameters of the model and also their variances, the resulted values of RSE and IIV for both SAL (control) and DEN/TAA (case) are acceptable. Accordingly, reaching such proper fittings was possible because the NLME framework is one of the most suitable approaches to handle population data with high variability [46].

The preceding results for k_1 are consistent with an analysis present in a paper regarding the MNP circulation time using first-order kinetics based on simply half-life $T_{1/2}$ [9]. With statistical significance, the initial study reports a decrease in MNP circulation time for DEN/TAA

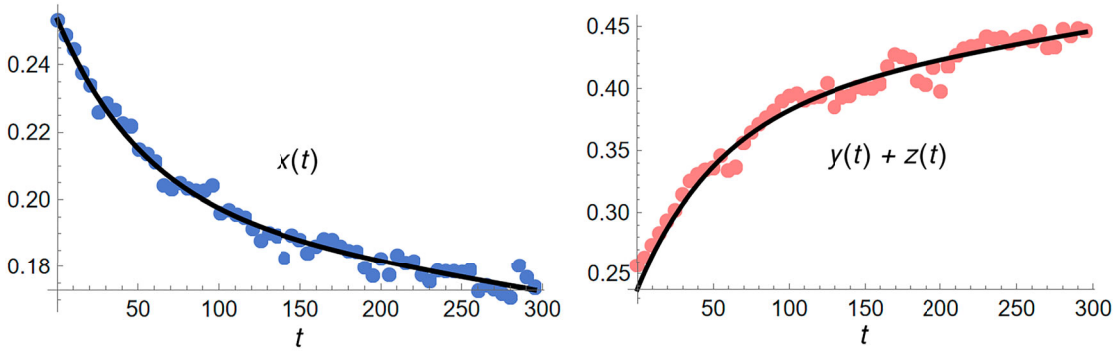

Figure 3. One of the many individual fittings of the model: curves of $x(t)$ and $y(t) + z(t)$ for the MNP amount vs. t (in seconds) compared against the respective experimental data.

Table 1. Parameter estimates with standard errors, relative standard errors (RSE), and inter-individual variability (IIV).

Parameter	Units	SAL Group				DEN/TAA Group			
		Estimate	Standard Error	RSE (%)	IIV (%)	Estimate	Standard Error	RSE (%)	IIV (%)
k_1	1/s	0.01008050	0.00253781	25.2	42.5	0.0159079	0.00840803	52.8	57.9
k_2	1/s	0.00537034	0.00126835	23.6	77.9	0.0138524	0.00678912	49.1	78.6
k_3	1/s	0.00041223	0.00021765	52.8	103.4	0.0021632	0.00059806	27.6	26.2
V_R	–	1.08015000	0.00838395	0.77	97.8	1.1405000	0.01986210	1.74	84.7

Notes: The latter was approximately computed as the square root of the diagonal entries of the population covariance matrix Ω.

group ($T_{1/2} = 11.2 \pm 3.1$ minutes) in comparison to the SAL group ($T_{1/2} = 19.6 \pm 2.3$ minutes). This shorter circulation half-life of MNP in DEN/TAA is consistent with a higher value of k_1 for this group reported in Table 1.

Regarding k_2, it defines how quickly the MNPs are transferred from the liver to circulating blood, and then to the heart. That being, our results suggest that the liver in a cirrhosis-induced process exchanges a higher amount of blood, resulting in more intensive MNP exchange. Regarding k_3, it defines the rate at which MNPs are irreversibly transferred from the liver compartment to a subcompartment within this organ [22]. Based on this parameter, our results indicate a faster absorption of MNPs by the liver for which the process of hepatocarcinogenesis has been started.

To further analyze our results for k_3, we related them to a classical pharmacokinetic analysis presented in the other paper in which the time to the highest MNP level at the liver T_{max} was reported [9]. It is observed that livers undergoing cirrhosis exhibited a lower peak of MNP attained in a shorter time ($T_{max} = 16.7 \pm 1.1$ minutes) in comparison with healthy livers ($T_{max} = 26.6 \pm 0.5$ minutes). Our pharmacokinetic modeling reveals higher values for k_3, explaining why cirrhotic livers exhibited a quicker MNP saturation than healthy livers, probably because in the former the Kupffer cells are more likely to MNP absorption.

4. Discussion

Mathematical models are essential for predicting and understanding complex phenomena such as nanoparticle interactions with living systems [47, 48]. They can provide predictive capabilities for rational product design and descriptive insights into underlying mechanisms. Sometimes a more detailed incorporation of complex underlying processes is mandatory to achieve a more robust modeling for a certain purpose [22]. At other times, however, the use of simple models is required to offer valuable insights or useful descriptions through calibration with available experimental data [24]. The understanding of the interaction mechanisms of magnetic nanoparticles with liver structures and how their uptake occurs is crucial for developing effective therapies. Mathematical models can help to illuminate these mechanisms by providing a useful and relevant framework for analyzing and interpreting experimental data [49, 50].

The modeling framework proposed in this research study provides a suitable description to quantitatively describe the biodistribution of MNPs in healthy and cirrhotic rats. Using a set of ordinary differential equations, the model allows for the estimation of transfer rates between compartments. The model's significance is primarily derived from its potential to inform the development of targeted drug-delivery strategies for treating and

diagnosing hepatocellular carcinoma [51]. Understanding how the condition of cirrhosis-associated hepatocarcinogenesis affects the biodistribution of MNPs may help interested researchers in designing more effective treatment protocols that maximize therapeutic efficacy while minimizing the risk of toxicity to healthy tissues [52]. In addition, the model may also have wider implications in the development of drug delivery systems, as it provides a useful framework for predicting the distribution and elimination of drugs or nanoparticles throughout the body [53]. Finally, it also provides a deeper analysis than the already reported MNPs biodistribution under a hepatic disease [9].

Regarding more specific aspects, we observe that during some pathological conditions such as chronic liver disease, liver sinusoidal endothelial cells (LSECs) undergo "capillarization," a process characterized by loss of fenestrations and acquisition of a vascular phenotype. Capillarization has been reported as an indicator of the fibrosis/cirrhosis process. Upon capillarization, the vanished fenestrae in LSECs significantly hinder substance exchange between the blood and liver cells. This could affect blood flow to hepatocytes [54–56].

The capillarization process can be related to our results once the value of k_2 is higher in the cirrhotic animals, indicating that the liver blood returns to the heart quickly. Since there was no extravasation to the hepatocytes, the blood tends to return to the heart more intensely. On the other hand, the value of k_3 is higher for cirrhotic animals, showing that MNP accumulates faster in Kupffer cells, which may be associated with an anticipated saturation process that cirrhosis induces in the liver due to the high blood flow that the liver receives [57].

When injected intravenously, magnetic nanoparticles (MNPs) are selectively taken up by the liver [58]. The liver is a complex organ composed of many different cell types that vary in both morphology and function, yet are closely interconnected. Liver cells can be divided into two major groups: parenchymal hepatocytes, which make up about 60–80% of the total number of liver cells, and non-parenchymal cells, which comprise approximately 20–40% of the total cells [49, 59].

In this context, it is interesting to question why the liver is the main target of nanoparticles. This aspect has been reviewed over the years by many researchers. Considering that the internalization process is influenced by the size of the nanoparticles as well as other properties such as charge. Generally, larger nanoparticles (with a diameter of 100–200 nm) demonstrate more efficient uptake by the liver [14, 60]. In addition, the main point is that after being part of the bloodstream and gaining access to the liver, there is a decrease in the speed of blood flow within the hepatic sinusoids [61–63]. This allows for intense interaction between hepatic structures, including Kupffer cells and hepatocytes, and blood [64]. It should be noted that resident macrophages in the liver are strategically positioned in the hepatic sinusoids, which favors this interaction between blood and these macrophagic structures.

Besides, the exposure of these nanoparticles to these different cells is not homogeneous. This is because the parenchymal part (mainly consisting of hepatocytes) is separated from the bloodstream by the hepatic sinusoids. These sinusoids have fenestrations ranging from 50 to 200 nanometers, which serve as a filter for nanoparticles smaller than 200 nanometers to access the space of Disse and have contact with the hepatocytes themselves [49, 64, 65]. Thus, some nanoparticles can pass through the hepatic sinusoids and return to the systemic circulation via the central vein [66, 67]. This may allow accumulation in other organs and tissues such as the spleen, lungs, tumor, etc. These released nanoparticles that escape from the liver can circulate and return to the liver to be captured by Kupffer cells.

It is known that during the cirrhosis process, the phenotype of the hepatic sinusoid changes drastically. Liver injury leads to endothelial dysfunction with loss of fenestrations and deposition of a basement membrane, a process known as capillarization. This process can significantly impair the exchange of substances between blood and hepatic cells [54, 68, 69]. This way, the data suggest that blood containing nanoparticles when accessing the damaged sinusoid (subjected to capillarization) did not allow these nanoparticles to reach the Disse space and the hepatocytes. They returned more quickly to the bloodstream compared to the healthy group, which is justified by the higher value of k_2.

It is worth pointing out that nanoparticles can interact with different liver cells, including hepatocytes and non-parenchymal cells, such as Kupffer cells. While non-parenchymal cells typically take up most nanoparticles, particles that interact with hepatocytes can be cleared from the body via the hepatobiliary pathway [70, 71]. Typically, nanoparticles with a diameter less than 150 nm can evade capture by Kupffer cells and pass through the fenestrations in the sinusoids, reaching the Disse space [72].

The liver sinusoids and intrahepatic blood flow dynamics are thought to direct particle extravasation from the liver sinusoids to the parenchymal regions through two processes: "forced sieving" and "endothelial massaging." Forced sieving happens when erythrocytes, which are soft and fast-moving, pass through narrow sinusoids and promote the entrance of fluid, solid-phase droplets, or particles such as chylomicrons into the space of Disse. Endothelial massaging happens when white blood cells,

which are rigid, pass through narrow sinusoids and compress the space of Disse, causing displacement of fluid [73, 74]. These processes were demonstrated by Wisse et al. [75] using in vivo microscopy to observe the interaction between blood cells and the fenestrated sinusoidal wall. In addition to both processes which act to blood extravasation to a parenchymal portion of the liver (Disse space and hepatocytes), deep and superficial hepatic lymphatic vessels may play a role in returning particles not taken up by hepatocytes to the systemic circulation [76, 77]. Once this blood return is considered slower by the central vein, it would justify our k_2 lesser values for the healthy group. The nanoparticle's interaction with hepatocytes is size-dependent. While large nanoparticles are preferentially taken up by Kupffer Cells, hepatocytes endocytose small nanoparticles. Also, the hepatocytes present a much lower uptake rate than macrophages [78].

According to previous characterizations and studies of the magnetic nanoparticles (MNPs) used in our mathematical modeling, these particles exhibit a high affinity for uptake by Kupffer cells. This is primarily due to their appropriate size, which facilitates recognition and uptake [52, 79]. In addition, it has been demonstrated that the hydrodynamic size of these MNPs makes them more susceptible to corona protein formation during the opsonization process. When MNPs are exposed to a biological medium, they interact with the molecules present in that medium. These molecules can adsorb onto the surface of the nanoparticles, forming a coating known as the corona [80]. This corona is composed of various molecules, including ions, proteins, surfactants, and other biomolecules present in the surrounding medium [81, 82]. The formation of this protein layer indirectly influences the effective size of the MNPs. This layer can increase the hydrodynamic radius or apparent size of the MNP [83].

In association with the non-extravasation to Disse space and hepatocytes, the blood flow circulation within the hepatic tissue is affected during liver diseases such as cirrhosis. It is discussed that the speed of blood flow within the hepatic sinusoids decreases as the diameter of the hepatic sinusoids becomes smaller [63]. Thus, we believe that the data are in line with this perspective of hemodynamic alteration that occurs during liver diseases, since the process of capillarization acts by blocking and closing the fenestrations that were previously present in the sinusoids. This phenomenon would be responsible for justifying the higher value of k_3 found for cirrhotic animals. Since the blood did not extravasate and reach the hepatocytes, it decreased its speed and could interact much more intensely with the Kupffer cells, being captured and retained in the hepatic tissue.

5. Concluding remarks

This study highlights the relevance of mathematical modeling for understanding complex phenomena such as nanoparticle interactions with living systems, particularly in developing effective therapies for cirrhosis-associated hepatocellular carcinoma. The proposed modeling approach provides a powerful tool to quantitatively describe the biodistribution of magnetic nanoparticles in healthy and cirrhotic rats, allowing for the estimation of pharmacokinetic rate parameters regarding the distribution of the magnetic nanoparticles. This achievement was made possible by employing an innovative experimental technique that provided relevant physiological data for the mathematical model.

Besides providing an accurate description of the concentration of nanoparticles in the liver and heart compartments over time, which may assist the development of targeted drug-delivery strategies, our modeling results suggest that the cirrhotic liver presents a higher blood flow than the healthy liver, which can be attributed to the elevated mass and high blood pressure in the veins that supply the liver, known as portal hypertension. Furthermore, the capillarization process, characterized by loss of fenestrations and acquisition of a vascular phenotype in liver sinusoidal endothelial cells, could affect blood flow to hepatocytes and may be associated with the observed differences in pharmacokinetic rates of nanoparticles in Kupffer cells. Finally, this study provides complementary insight into the biodistribution of magnetic nanoparticles under hepatic disease and demonstrates the potential of mathematical models for analyzing and interpreting experimental data in developing drug delivery systems, also contributing to their development in theranostic applications.

Acknowledgments

DSR is thankful to Carmen Molina-Paris and Veronika Zarnitsyna for valuable discussions on this work that took place in 2022 at ICTP-SAIFR QBio Program, São Paulo, Brazil.

Disclosure statement

No potential conflict of interest was reported by the author(s).

Funding

DSR, JRAM, VAGL, ATB, and GAS thanks the funding received from FAPESP (Grant #2020/05556-0 and Grant #2021/06405-9, São Paulo Research Foundation). JRAM also thanks CNPq and INCT-FNA.

ORCID

Diego S. Rodrigues http://orcid.org/0000-0002-0016-1715
Guilherme A. Soares http://orcid.org/0000-0002-4723-466X

Verónica A. González-López http://orcid.org/0000-0002-3514-4130
Anibal T. Bezerra http://orcid.org/0000-0001-9758-0117
Mats Jirstrand http://orcid.org/0000-0002-6612-8037
José R. A. Miranda http://orcid.org/0000-0002-8306-8056

References

[1] Arsalani S, Löwa N, Kosch O, et al. Magnetic separation of iron oxide nanoparticles to improve their application for magnetic particle imaging. Phys Med Biol. 2021;66(1):015002. doi: 10.1088/1361-6560/abcd19
[2] Avasthi A, Caro C, Pozo-Torres E, et al. Magnetic nanoparticles as MRI contrast agents. Topics Curr Chem. 2020;378(3):1–43. doi:10.1007/s41061-020-00302-w.
[3] Haghighi AH, Khorasani MT, Faghih Z, et al. Effects of different quantities of antibody conjugated with magnetic nanoparticles on cell separation efficiency. Heliyon. 2020;6(4):e03677. doi: 10.1016/j.heliyon.2020.e03677
[4] Miranda JR, Baffa O, de Oliveira RB, et al. An AC biosusceptometer to study gastric emptying. Med Phys. 1992;19(2):445–448. doi: 10.1118/1.596832
[5] Quini CC, Próspero AG, Calabresi MF, et al. Real-time liver uptake and biodistribution of magnetic nanoparticles determined by AC biosusceptometry. Nanomed Nanotechnol Biol Med. 2017;13(4):1519–1529. doi: 10.1016/j.nano.2017.02.005
[6] Próspero AG, Quini CC, Bakuzis AF, et al. Real-time in vivo monitoring of magnetic nanoparticles in the bloodstream by AC biosusceptometry. J Nanobiotechnol. 2017;15(1):1–12. doi: 10.1186/s12951-017-0257-6.
[7] Prospero AG, de Oliveira PF, Soares GA, et al. AC biosusceptometry and magnetic nanoparticles to assess doxorubicin-induced kidney injury in rats. Nanomedicine. 2020;15(5):511–525. doi: 10.2217/nnm-2019-0300
[8] Soares GA, Prospero AG, Calabresi MF, et al. Multichannel AC biosusceptometry system to map biodistribution and assess the pharmacokinetic profile of magnetic nanoparticles by imaging. IEEE Trans Nanobioscience. 2019;18(3):456–462. doi: 10.1109/tnb.2019.2912073
[9] Soares GA, Pereira GM, Romualdo GR, et al. Biodistribution profile of magnetic nanoparticles in cirrhosis-associated hepatocarcinogenesis in rats by AC biosusceptometry. Pharmaceutics. 2022;14(9):1907. doi: 10.3390/pharmaceutics14091907
[10] Soares GA, Faria JVC, Pinto LA, et al. Long-term clearance and biodistribution of magnetic nanoparticles assessed by AC biosusceptometry. Materials. 2022;15(6):2121. doi: 10.3390/ma15062121
[11] Li Y, Shang W, Liang X, et al. The diagnosis of hepatic fibrosis by magnetic resonance and near-infrared imaging using dual-modality nanoparticles. RSC Adv. 2018;8(12):6699–6708. doi: 10.1039/c7ra10847h
[12] Saraswathy A, Nazeer SS, Nimi N, et al. Asialoglycoprotein receptor targeted optical and magnetic resonance imaging and therapy of liver fibrosis using pullulan stabilized multi-functional iron oxide nanoprobe. Sci Rep. 2021;11(1):1–11. doi: 10.1038/s41598-021-97808-0.
[13] Nagórniewicz B, Mardhian DF, Booijink R, et al. Engineered relaxin as theranostic nanomedicine to diagnose and ameliorate liver cirrhosis. Nanomed Nanotechnol Biol Med. 2019;17:106–118. doi: 10.1016/j.nano.2018.12.008
[14] Levada K, Omelyanchik A, Rodionova V, et al. Magnetic-assisted treatment of liver fibrosis. Cells. 2019 Oct;8(10):1279. doi: 10.3390/cells8101279
[15] Shreyash N, Bajpai S, Khan MA, et al. Green synthesis of nanoparticles and their biomedical applications: A review. ACS Appl Nano Mater. 2021;4(11):11428–11457. doi: 10.1021/acsanm.1c02946
[16] Yu Z, Gao L, Chen K, et al. Nanoparticles: A new approach to upgrade cancer diagnosis and treatment. Nanoscale Res Lett. 2021;16(1):1–17. doi: 10.1186/s11671-021-03489-z.
[17] Yao Y, Zhou Y, Liu L, et al. Nanoparticle-based drug delivery in cancer therapy and its role in overcoming drug resistance. Front Mol Biosci. 2020;7:1–14. doi: 10.3389/fmolb.2020.00193.
[18] Patra JK, Das G, Fraceto LF, et al. Nano based drug delivery systems: recent developments and future prospects. J Nanobiotechnol. 2018;16(1):1–33. doi: 10.1186/s12951-018-0392-8.
[19] Li J, Tuo B. Current and emerging approaches for hepatic fibrosis treatment. Gastroenterol Res Pract. 2021;2021:1–13. doi: 10.1155/2021/6612892
[20] Sun T, Kang Y, Liu J, et al. Nanomaterials and hepatic disease: toxicokinetics, disease types, intrinsic mechanisms, liver susceptibility, and influencing factors. J Nanobiotechnolog. 2021;19(1):1–33. doi: 10.1186/s12951-021-00843-2.
[21] Shin HK, Kang YM, No KT. Predicting ADME properties of chemicals. In: Handbook of computational chemistry. Cham: Springer International Publishing; 2017. p. 2265–2301. doi: 10.1007/978-3-319-27282-5_59
[22] Dogra P, Butner JD, Ramırez JR, et al. A mathematical model to predict nanomedicine pharmacokinetics and tumor delivery. Comput Struct Biotechnol J. 2020;18:518–531. doi: 10.1016/j.csbj.2020.02.014
[23] Sousa-Junior A, Yang CT, Korangath P, et al. A predictive pharmacokinetic model for immune cell-mediated uptake and retention of nanoparticles in tumors. Int J Mol Sci. 2022;23(24):15664. doi: 10.3390/ijms232415664
[24] Čelechovská L. A simple mathematical model of the human liver. Appl Math. 2004;49(3):227–246. doi: 10.1023/b:apom.0000042364.85016.7d
[25] Baleanu D, Jajarmi A, Mohammadi H, et al. A new study on the mathematical modelling of human liver with caputo-fabrizio fractional derivative. Chaos Solitons Fract. 2020;134:109705. doi: 10.1016/j.chaos.2020.109705
[26] Berglund M, Sunnaker M, Adiels M, et al. Investigations of a compartmental model for leucine kinetics using non-linear mixed effects models with ordinary and stochastic differential equations. Math Med Biol. 2011;29(4):361–384. doi: 10.1093/imammb/dqr021
[27] Narsinh KH, Cui J, Papadatos D, et al. Hepatocarcinogenesis and LI-RADS. Abdominal Radiolog. 2017 Dec;43(1):158–168. doi: 10.1007/s00261-017-1409-8.
[28] Romualdo GR, Grassi TF, Goto RL, et al. An integrative analysis of chemically-induced cirrhosis-associated hepatocarcinogenesis: Histological, biochemical and molecular features. Toxicol Lett. 2017 Nov;281:84–94. doi: 10.1016/j.toxlet.2017.09.015.
[29] Kerdput V, Kanjanapongkul K, Itharat A, et al. Molecular changes following induction of hepatocellular carcinoma by diethylnitrosamine and thioacetamide, and subsequent treatment with dioscorea membranacea extract. Int J Med Sci. 2022;19(12):1806–1815. doi: 10.7150/ijms.72987.

[30] Henderson JM, Polak N, Chen J, et al. Multiple liver insults synergize to accelerate experimental hepatocellular carcinoma. Sci Rep. 2018 Jul;8(1):1–12. doi: 10.1038/s41598-018-28486-8.
[31] Memon A, Pyao Y, Jung Y, et al. A modified protocol of diethylnitrosamine administration in mice to model hepatocellular carcinoma. Int J Mol Sci. 2020 Jul;21(15):5461. doi: 10.3390/ijms21155461.
[32] Kurma K, Manches O, Chuffart F, et al. Den-induced rat model reproduces key features of human hepatocellular carcinoma. Cancers. 2021 Oct;13(19):4981. doi: 10.3390/cancers13194981.
[33] Dwivedi DK, Jena G. Diethylnitrosamine and thioacetamide-induced hepatic damage and early carcinogenesis in rats: Role of nrf2 activator dimethyl fumarate and nlrp3 inhibitor glibenclamide. Biochem Biophys Res Commun. 2020 Feb;522(2):381–387. doi: 10.1016/j.bbrc.2019.11.100.
[34] Branquinho LC, Carrião MS, Costa AS, et al. Effect of magnetic dipolar interactions on nanoparticle heating efficiency: Implications for cancer hyperthermia. Sci Rep. 2013;3(1):1–10. doi: 10.1038/srep02887.
[35] Watt JM, Young A. An attempt to simulate the liver on a computer. Comput J. 1962;5(3):221–227. doi: 10.1093/comjnl/5.3.221
[36] Leander J, Almquist J, Johnning A, et al. NLMEModeling: a wolfram mathematica package for nonlinear mixed effects modeling of dynamical systems, arXiv:2011.06879; 2020.
[37] Olafsdottir HK, Leander J, Almquist J, et al. Exact gradients improve parameter estimation in nonlinear mixed effects models with stochastic dynamics. AAPS J. 2018;20(5):1–13. doi: 10.1208/s12248-018-0232-7.
[38] Almquist J, Leander J, Jirstrand M. Using sensitivity equations for computing gradients of the FOCE and FOCEI approximations to the population likelihood. J Pharmacokinet Pharmacodyn. 2015;42(3):191–209. doi: 10.1007/s10928-015-9409-1
[39] Karlsson J, Anguelova M, Jirstrand M. An efficient method for structural identifiability analysis of large dynamic systems. IFAC Proc Vol. 2012;45(16):941–946. doi: 10.3182/20120711-3-be-2027.00381
[40] Raue A, Karlsson J, Saccomani MP, et al. Comparison of approaches for parameter identifiability analysis of biological systems. Bioinformatics. 2014;30(10):1440–1448. doi: 10.1093/bioinformatics/btu006
[41] Anguelova M, Karlsson J, Jirstrand M. Minimal output sets for identifiability. Math Biosci. 2012;239(1):139–153. doi: 10.1016/j.mbs.2012.04.005
[42] Janzén DL, Jirstrand M, Chappell MJ, et al. Three novel approaches to structural identifiability analysis in mixed-effects models. Comput Methods Programs Biomed. 2019 Apr;171:141–152. doi: 10.1016/j.cmpb.2016.04.024
[43] Mould D, Upton R. Basic concepts in population modeling, simulation, and model-based drug development-part 2: Introduction to pharmacokinetic modeling methods. CPT: Pharmacomet Syst Pharmacol. 2013 Apr;2(4):38. doi: 10.1038/psp.2013.14
[44] Esdonk MJ, Lindeman I, Okkerse P, et al. Population pharmacokinetic/pharmacodynamic analysis of nociceptive pain models following an oral pregabalin dose administration to healthy subjects. CPT: Pharmacomet Syst Pharmacolog. 2018 Aug;7(9):573–580. doi: 10.1002/psp4.12318
[45] Brendel K, Bekaii-Saab T, Boland PM, et al. Population pharmacokinetics of liposomal irinotecan in patients with cancer and exposure–safety analyses in patients with metastatic pancreatic cancer. CPT: Pharmacomet Syst Pharmacolog. 2021 Nov;10(12):1550–1563. doi: 10.1002/psp4.12725
[46] Lindstrom MJ, Bates DM. Nonlinear mixed effects models for repeated measures data. Biometrics. 1990;46(3):673. doi: 10.2307/2532087
[47] Sahai N, Gogoi M, Ahmad N. Mathematical modeling and simulations for developing nanoparticle-based cancer drug delivery systems: A review. Curr Pathobiol Rep. 2021;9(1):1–8. doi: 10.1007/s40139-020-00219-5
[48] Gabrielsson J, Andersson K, Tobin G, et al. Maxsim2—real-time interactive simulations for computer-assisted teaching of pharmacokinetics and pharmacodynamics. Comput Methods Programs Biomed. 2014 Mar;113(3):815–829. doi: 10.1016/j.cmpb.2013.12.006
[49] Zhang YN, Poon W, Tavares AJ, et al. Nanoparticle–liver interactions: Cellular uptake and hepatobiliary elimination. J Control Release. 2016 Oct;240:332–348. doi: 10.1016/j.jconrel.2016.01.020
[50] Poon W, Kingston BR, Ouyang B, et al. A framework for designing delivery systems. Nat Nanotechnol. 2020;15(10):819–829. doi: 10.1038/s41565-020-0759-5
[51] Abza GB, Ahmed JH, Yesufe AA, et al. Clinicopathological features and survival of patients with hepatocellular carcinoma in ethiopia: A multicenter study. Cancers. 2022;15(1):193. doi: 10.3390/cancers15010193
[52] Ngo W, Ahmed S, Blackadar C, et al. Why nanoparticles prefer liver macrophage cell uptake in vivo. Adv Drug Deliv Rev. 2022 Jun;185:114238. doi: 10.1016/j.addr.2022.114238
[53] Rajoli RKR. Pharmacokinetic modelling to study the biodistribution of nanoparticles. In: Mucosal delivery of drugs and biologics in nanoparticles. Cham: Springer International Publishing; 2020. p. 247–267. doi: 10.1007/978-3-030-35910-2_11
[54] DeLeve LD. Liver sinusoidal endothelial cells in hepatic fibrosis. Hepatology. 2015;61(5):1740–1746. doi: 10.1002/hep.27376
[55] Ruan B, Duan JL, Xu H, et al. Capillarized liver sinusoidal endothelial cells undergo partial endothelial-mesenchymal transition to actively deposit sinusoidal ECM in liver fibrosis. Front Cell Dev Biol. 2021;9:1–14. doi: 10.3389/fcell.2021.671081.
[56] Ma H, Liu X, Zhang M, et al. Liver sinusoidal endothelial cells are implicated in multiple fibrotic mechanisms. Mol Biol Rep. 2021;48(3):2803–2815. doi: 10.1007/s11033-021-06269-1
[57] Gracia-Sancho J, Marrone G, Fernández-Iglesias A. Hepatic microcirculation and mechanisms of portal hypertension. Nat Rev Gastroenterolog Hepatolog. 2018;16(4):221–234. doi: 10.1038/s41575-018-0097-3
[58] Cole AJ, Yang VC, David AE. Cancer theranostics: the rise of targeted magnetic nanoparticles. Trends Biotechnol. 2011 Jul;29(7):323–332. doi: 10.1016/j.tibtech.2011.03.001
[59] Park JK, Utsumi T, Seo YE, et al. Cellular distribution of injected PLGA-nanoparticles in the liver. Nanomed Nanotechnolog Biol Med. 2016 Jul;12(5):1365–1374. doi: 10.1016/j.nano.2016.01.013

[60] Colino CI, Lanao JM, Gutierrez-Millan C. Targeting of hepatic macrophages by therapeutic nanoparticles. Front Immunol. 2020 Mar;11:1–17. doi: 10.3389/fimmu.2020.00218.
[61] Yao H, Wang Y. Relationship between hemodynamic parameters and portal venous pressure in cirrhosis patients with portal hypertension. Open Life Sci. 2020 Dec;15(1):981–987. doi: 10.1515/biol-2020-0101
[62] Chen YY, Syed AM, MacMillan P, et al. Flow rate affects nanoparticle uptake into endothelial cells. Adv Mater. 2020 May;32(24):1906274. doi: 10.1002/adma.201906274
[63] Fan J, Chen CJ, Wang YC, et al. Hemodynamic changes in hepatic sinusoids of hepatic steatosis mice. World J Gastroenterol. 2019 Mar;25(11):1355–1365. doi: 10.3748/wjg.v25.i11.1355
[64] Zhang LF, Wang XH, Zhang CL, et al. Sequential nanopenetrators of capillarized liver sinusoids and extracellular matrix barriers for liver fibrosis therapy. ACS Nano. 2022 Aug;16(9):14029–14042. doi: 10.1021/acsnano.2c03858
[65] Nowak-Jary J, Machnicka B. Pharmacokinetics of magnetic iron oxide nanoparticles for medical applications. J Nanobiotechnolog. 2022 Jun;20(1):1–30. doi: 10.1186/s12951-022-01510-w.
[66] Wang H, Thorling CA, Liang X, et al. Diagnostic imaging and therapeutic application of nanoparticles targeting the liver. J Mater Chem B. 2015;3(6):939–958. doi: 10.1039/c4tb01611d
[67] Mîndrilă B, Buteică SA, Mîndrilă I, et al. Administration routes as modulators of the intrahepatic distribution and anti-anemic activity of salicylic acid/Fe_3O_4 nanoparticles. Biomedicines. 2022 May;10(5):1213. doi: 10.3390/biomedicines10051213
[68] Baiocchini A, Nonno FD, Taibi C, et al. Liver sinusoidal endothelial cells (LSECs) modifications in patients with chronic hepatitis c. Sci Rep. 2019 Jun;9(1):1–10. doi: 10.1038/s41598-019-45114-1.
[69] Greuter T, Shah VH. Hepatic sinusoids in liver injury, inflammation, and fibrosis: new pathophysiological insights. J Gastroenterol. 2016 Mar;51(6):511–519. doi: 10.1007/s00535-016-1190-4
[70] Yu M, Zheng J. Clearance pathways and tumor targeting of imaging nanoparticles. ACS Nano. 2015 Jul;9(7):6655–6674. doi: 10.1021/acsnano.5b01320
[71] Poon W, Zhang YN, Ouyang B, et al. Elimination pathways of nanoparticles. ACS Nano. 2019 Apr;13(5):5785–5798. doi: 10.1021/acsnano.9b01383
[72] Jiang L, Wang T, Wang Y, et al. Co-disposition of chitosan nanoparticles by multi types of hepatic cells and their subsequent biological elimination: the mechanism and kinetic studies at the cellular and animal levels. Int J Nanomedicine. 2019 Jul;14:6035–6060. doi: 10.2147/ijn.s208496
[73] Moghimi SM, McCullough R, Simberg D. Revisiting nano particle transendothelial migration in the liver. Mol Ther. 2023 Mar;31(3):605–606. doi: 10.1016/j.ymthe.2023.01.024
[74] Haroon H, Hunter A, Farhangrazi Z, et al. A brief history of long circulating nanoparticles. Adv Drug Deliv Rev. 2022 Sep;188:114396. doi: 10.1016/j.addr.2022.114396
[75] Wisse E, de Zanger RB, Charels K, et al. The liver sieve: Considerations concerning the structure and function of endothelial fenestrae, the sinusoidal wall and the space of disse. Hepatology. 1985 Jul;5(4):683–692. doi: 10.1002/hep.1840050427
[76] Ohtani O, Ohtani Y. Lymph circulation in the liver. Anat Rec Adv Integr Anat Evol Biol. 2008;291(6):643–652. doi: 10.1002/ar.20681
[77] Tanaka M, Iwakiri Y. The hepatic lymphatic vascular system: Structure, function, markers, and lymphangiogenesis. Cell Mol Gastroenterol Hepatol. 2016 Nov;2(6):733–749. doi: 10.1016/j.jcmgh.2016.09.002
[78] Haute DV, Berlin JM. Challenges in realizing selectivity for nanoparticle biodistribution and clearance: lessons from gold nanoparticles. Ther Deliv. 2017 Aug;8(9):763–774. doi: 10.4155/tde-2017-0057
[79] Walkey CD, Olsen JB, Guo H, et al. Nanoparticle size and surface chemistry determine serum protein adsorption and macrophage uptake. J Am Chem Soc. 2012 Jan;134(4):2139–2147. doi: 10.1021/ja2084338
[80] Cedervall T, Lynch I, Foy M, et al. Detailed identification of plasma proteins adsorbed on copolymer nanoparticles. Angew Chem Int Ed. 2007 Jul;46(30):5754–5756. doi: 10.1002/anie.200700465
[81] Rampado R, Crotti S, Caliceti P, et al. Recent advances in understanding the protein corona of nanoparticles and in the formulation of "stealthy" nanomaterials. Front Bioeng Biotechnol. 2020 Apr;8:1–19. doi: 10.3389/fbioe.2020.00166.
[82] Kopac T. Protein corona, understanding the nanoparticle–protein interactions and future perspectives: A critical review. Int J Biol Macromol. 2021 Feb;169:290–301. doi: 10.1016/j.ijbiomac.2020.12.108
[83] Prospero AG, Buranello LP, Fernandes CA, et al. Corona protein impacts on alternating current biosusceptometry signal and circulation times of differently coated $MnFe_2O_4$ nanoparticles. Nanomedicine. 2021 Oct;16(24):2189–2206. doi: 10.2217/nnm-2021-0195